

# Temperature-dependent performance of amorphous silicon photovoltaic/thermal systems in the long term operation

Xiao Ren<sup>a</sup>, Jing Li<sup>b,\*</sup>, Dongsheng Jiao<sup>a</sup>, Datong Gao<sup>a</sup>, Gang Pei<sup>a,\*</sup>

<sup>a</sup> *Department of Thermal Science and Energy Engineering, University of Science and Technology of China, 96 Jinzhai Road, Hefei, China*

<sup>b</sup> *Research Center for Sustainable Energy Technologies, Energy and Environment Institute, University of Hull, Hull, HU6 7RX, UK*

\*Corresponding author. Tel. /Fax: [lijing83@ustc.edu.cn](mailto:lijing83@ustc.edu.cn) +86 551 63607517; [peigang@ustc.edu.cn](mailto:peigang@ustc.edu.cn) +86 551 63607367

## Abstract:

The influences of temperature on the performance of amorphous silicon (a-Si) solar cells and photovoltaic (PV) systems are extensively studied in the literature. The benefit from thermal annealing effect at a higher temperature than ambient has been demonstrated, which makes a-Si cells a promising material for photovoltaic/thermal (PV/T) system. However, the temperature-dependent performance of a-Si PV/T system in the long term operation has rarely been reported. The temperature effect will be more complicated than that on a single cell or PV system. Particularly, the exergetic efficiency and mechanical behavior of the PV/T system at different temperatures are unknown. To fill the above knowledge gap, two identical a-Si PV/T systems are developed. One operates at a water inlet temperature of 60 °C with an a-Si cell temperature of up to 70 °C. The other operates at an inlet temperature of 30 °C. Long-term outdoor tests from December 2017 to June 2019 have been conducted. Results indicate that the difference in the electrical efficiency between the two systems is

0.47% in the initial stage, and it gradually narrows to only 0.13% over time. The overall exergy efficiency at 60 °C generally exceeds that at 30 °C, which proves the superiority of the a-Si PV/T operating at medium temperature. Besides, the long-term operation at 60 °C has not led to a lower level of reliability.

**Keywords:** Amorphous silicon cells, Photovoltaic/thermal, Temperature, Long-term experiments, Energy efficiency, Exergy efficiency.

## 1. Introduction

Photovoltaic/Thermal (PV/T) systems generate both heat and power, offering an increasingly popular solar option. The number of PV/T systems in operation has reached more than 22,000 in 2018 [1]. However, one challenge for the mainstream PV/T systems using crystalline silicon (c-Si) cells is the significant decrement of electricity with the increase of operation temperature. The PV/T systems may not have advantages over side-by-side PV and solar thermal collector systems, especially in the medium-high temperature ranges. Amorphous silicon (a-Si) cell is an alternative photovoltaic (PV) material for the PV/T system [2]. Due to the low power temperature coefficient of a-Si cells ( $-0.1$  to  $-0.2$  %/°C), it exhibits a relatively small variation in efficiency with increasing cell temperature [3], as compared with the high power temperature coefficient of c-Si cells ( $-0.4$  to  $-0.5$  %/°C) [4, 5]. Moreover, the long-term performance indicated that a-Si cells may have a positive power temperature coefficient [6, 7], which indeed is a highly advantageous feature for PV/T systems at medium-high temperatures [8, 9]. The temperature of the a-Si cells plays an important role in the process of light-induced degradation [10], whilst the thermal energy and useful energy are greatly affected by the operating temperature in PV/T systems.

Nomenclature		
$A$	area, m <sup>2</sup>	<i>Subscripts</i>
$c$	specific heat capacity, J/kg·K	a average
$\dot{E}_x$	exergy, W	air ambient, air
$FF$	fill factor	c collector
$G$	solar irradiation, W/m <sup>2</sup>	ex exergy
$h$	heat transfer coefficient, W/m <sup>2</sup> ·K	$G$ solar irradiation
$H$	total solar irradiance, J/m <sup>2</sup> , MJ/m <sup>2</sup>	in inlet of collector
$I$	current, A	loss energy loss
$\dot{m}$	mass flow rate, kg/s	m mean
$P$	Power, W, MJ	mp maximum power
$Q$	energy, W, MJ	oc open-circuit
$R$	thermal resistance, m <sup>2</sup> ·K /W	out outlet of collector
$T$	temperature, K	pv PV module
$U$	voltage, V	pvt PV/T
$U_{\text{loss}}$	energy loss coefficient of system, MJ/m <sup>2</sup> ·K	sc short-circuit
		sun solar
		t total
<i>Greek letters</i>		th thermal
$\eta$	efficiency	w water
$\zeta$	covering factor	0 zero

At present, the effect of temperature on single a-Si solar cells and a-Si PV systems has been extensively investigated. The controlled light-soaking tests on a-Si cells at different temperatures indicated that cycling and changing the exposure temperature modified the efficiency of a-Si cells between 10% and 17% in a recurrent pattern [11]. The a-Si cells could reach higher stabilized efficiencies at higher operating temperatures and the stabilized performance levels depended largely on light exposure and a characteristic temperature [12, 13]. Moreover, higher temperatures resulted in faster degradation in the early stages of the degenerated process [14]. The a-Si cells exhibited relatively little temperature dependence when they were operating in equilibrium, but a relatively strong temperature dependence in a short period of time [15]. Besides, the history of creation and annealing of light-induced defect states were important for determining the subsequent kinetics of creation and

annealing [16]. Thus, the operating temperature during light-soaking was deemed as the most important factor for determining the stabilized performance of a-Si cells.

The above researches are only related to single solar cells and focus on the electric performance. However, it is difficult to predict the temperature-dependent performance of a-Si PV/T system, especially in a long term operation. The reasons are as follows.

I. Experimental data are lacked. The Staebler–Wronski (S-W) and thermal annealing effects generally take six or more months to reach an equilibrium. It may be longer in the PV/T application owing to the fluctuation of the operating temperature. To the best of the authors' knowledge, an experimental study on the long-term effect of temperature on the a-Si PV/T system has yet to be reported. In fact, longstanding evidential data are lacking even for the mainstream PV/T systems using c-Si cells [17, 18]. Long-term performance is one of the most important research directions of the PV/T system in the future [19].

II. Unlike the situation of sole PV generation, the operation temperature of a-Si PV/T system not only affects the electric output but also the thermodynamic performance. Thermal efficiency is an important index in the evaluation of a PV/T system, whilst the operating temperature has an essential effect on it [20]. In the aforementioned studies of temperature impact on a-Si cells, the thermal conversion is not considered and the conclusions may not be applicable for the utilization of solar heat.

III. The mechanical behavior of a-Si PV/T system depends on the temperature profile on the components. Solar cells are normally laminated on a metal absorber e.g., aluminum to enhance heat transfer. The PV/T system is vulnerable to thermal stress due to the temperature gradients and significant differences in the thermal expansion coefficients of the absorber and solar cells [21]. Breakdown of mechanical structure can happen especially when the temperature fluctuation is large.

1 In addition, the PV/T systems generally operate in recurrent alternating heating and cooling conditions  
2  
3 [22]. The PV/T temperature is high during the day time while low at night. The periodic thermal stress  
4  
5 increases the possibility of fracture.  
6  
7

8  
9 IV. For a PV/T collector such as a flat-plate type, the working fluid temperature along the flow  
10  
11 direction is gradually increasing, resulting in non-uniform temperature distribution. Such distribution  
12  
13 across the PV cells in series or parallel lead to unpredictable electric performance, as well as thermal  
14  
15 stresses [23, 24]. The effect of temperature on an a-Si PV/T system is more complicated than that on  
16  
17 a PV system.  
18  
19

20  
21 V. Previous studies on the temperature effects were mainly conducted at indoor laboratories through  
22  
23 solar simulators. The natural environment, such as the solar spectrum, ambient temperature, and  
24  
25 humidity, cannot be accurately simulated in laboratories. There is a certain difference between using  
26  
27 solar simulators and natural environments to measure the electrical performance of the PV module.  
28  
29 For example, some works have shown that the electrical efficiency of a-Si cells was subject to seasonal  
30  
31 variations [25]; it was higher in summer and lower in winter due to the spectral effects, light-induced  
32  
33 annealing or thermal annealing [26, 27]. Indeed, it would be difficult to simulate such seasonal  
34  
35 variations by the solar simulators inside the laboratories. Hence, it is necessary to conduct experimental  
36  
37 research in the natural environment.  
38  
39  
40  
41  
42  
43  
44  
45  
46

47 Above all, operating temperature is a crucial parameter of a PV/T system. Despite the potential of  
48  
49 a-Si cells in the PV/T application, it is unknown whether the system will exhibit better performance at  
50  
51 a higher temperature under real operating conditions. The present work aims to fill the gap of  
52  
53 knowledge on the temperature-independent performance of the a-Si PV/T system. The novelty and  
54  
55 contribution are:  
56  
57  
58  
59

- (1) Two identical prototypes are developed. It is the first time that the performance of a-Si PV/T system in the long-term operation is compared at two levels of temperature.
- (2) Continuous real-time performance of the prototypes from December 2017 to June 2019 has been monitored. Experimental data on the heat and power efficiencies as well as thermodynamic properties over the period are provided.
- (3) The difference between the temperature impacts on a-Si PV/T and c-Si PV/T systems is highlighted and explained.
- (4) Mechanical influence by temperature is clarified via direct and indirect detection of the structure of the a-Si PV/T systems after the long-term operation.

## 2. Methodology

### 2.1 Materials and structure

The a-Si cells used in the PV/T system are provided by Xunlight (Kunshan) Co., Ltd [28]. As shown in Fig. 1, the triple-junction thin-film solar cells are composed of the a-Si cell, a-Si germanium (a-SiGe) cell and a-SiGe cell from top to bottom with the substrate of stainless steel plate. Each layer absorbs the solar spectrum at different wave-bands as shown in Fig. 2 (a). The peak quantum efficiencies of top a-Si cell, middle a-SiGe cell, and bottom a-SiGe cell are about 67% at 450nm, 55% at 580 nm and 48% at 710 nm, respectively, and the total quantum efficiency can reach up to 86% at 570 nm. This structure enables a wider spectrum conversion ability of light into electricity than conventional a-Si modules. The emissivity/absorptivity of the triple-junction a-Si cells is presented in Fig. 2 (b). The a-Si cells exhibit high absorptivity in the spectral response bands between 380 nm and 980 nm. The initial efficiency and fill factor (FF) at the standard test condition each are 7.64% and

61%.

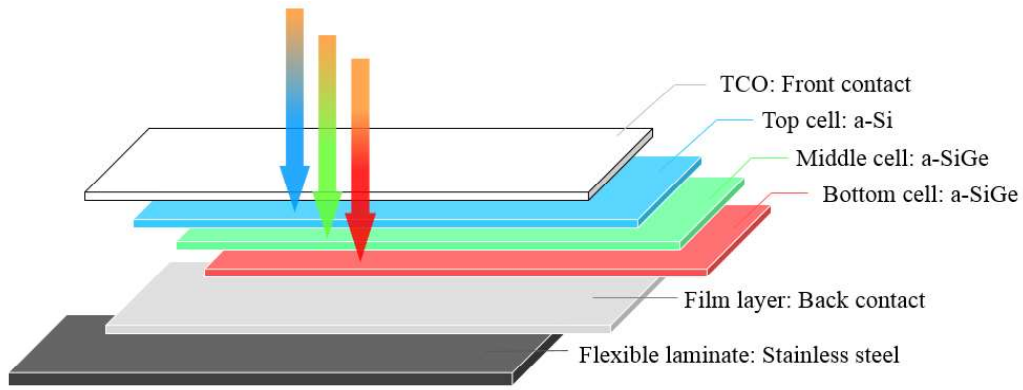


Fig. 1 Structure of the triple-junction a-Si cells.

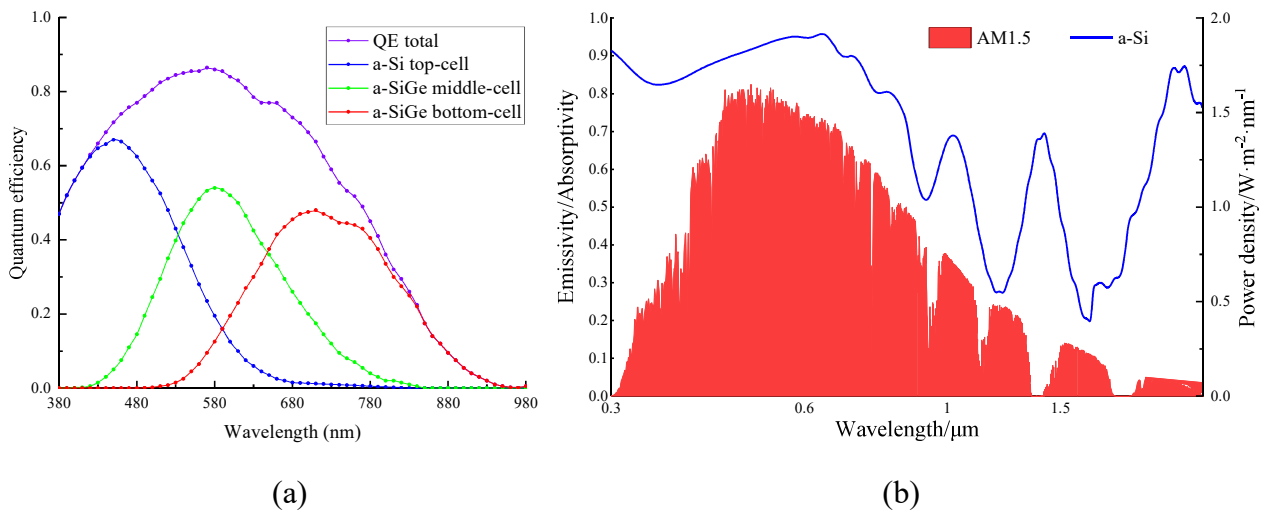


Fig. 2. Emissivity/absorptivity and quantum efficiency of the triple-junction a-Si cells.

The structure of the a-Si PV/T collector is shown in Fig. 3. The a-Si PV/T collector consists of the following components from top to bottom: glass cover, a-Si cells, aluminum absorber plate, copper tubes, insulating layer, and back plate. Fifteen a-Si cells are laminated onto the absorber plate through the adhesive layer (black Tedlar-polyester-Tedlar and ethylene-vinyl-acetate). To reduce the heat loss, an air gap is set between the glass cover and the a-Si cells, and an insulating layer is employed on the bottom of the a-Si PV/T collector. There are seven copper tubes and two water collector pipes welded on the back of the absorber plate.

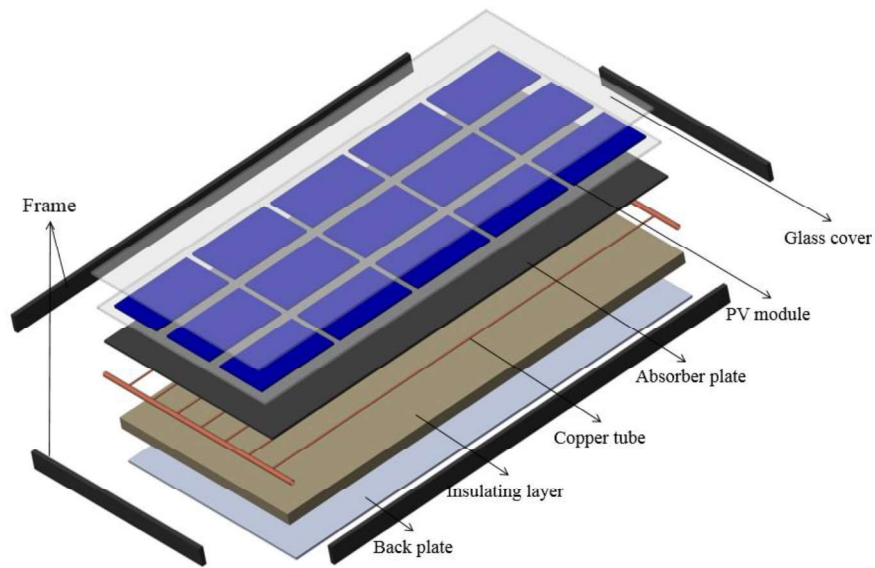


Fig. 3 Structure of the a-Si PV/T collector.

## 2.2 Experimental methods

To investigate the temperature-dependent performance, two a-Si PV/T systems are operated at a low water inlet temperature of 30 °C and a medium one of 60 °C, respectively. The actual setup and the schematic diagram of the two systems are depicted in Fig. 4 and Fig. 5. The inlet water temperature is controlled by the thermostatic water tank (DC-0515), so that the systems can operate at a stable temperature. Maximum power point tracking solar charge controllers are employed to track the current and voltage at the maximum power point. The two systems are running at 30 °C and 60 °C during day time, but turn off and cool down at night.



Fig. 4. Actual setup of two a-Si PV/T systems.

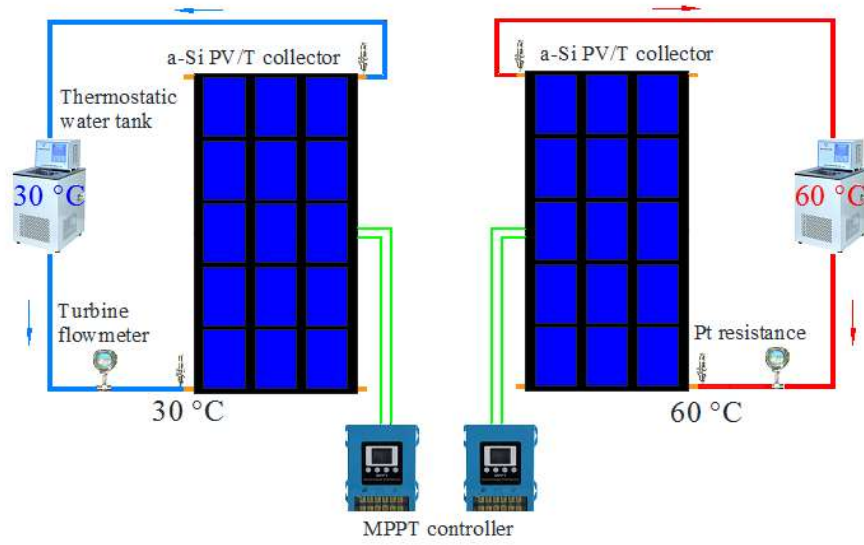


Fig. 5. Schematic diagram of two a-Si PV/T systems.

### 2.3 Performance analysis

The first-law (energy) and second-law (exergy) thermodynamic analyses are used to investigate the long-term performance of a-Si PV/T system under different operating temperatures. Based on the first law of thermodynamics, the thermal and electrical energy is only evaluated and compared under a metric standard without reference to the actual thermodynamic properties. Exergy measures the maximum useful work in a process that achieves a complete equilibrium between the system and the environment. The second law of thermodynamics can assess the quality of each energy flux, which is significant for system performance analysis.

#### 2.3.1 First-law analysis

The thermal performance is evaluated by the heat gain and thermal efficiency. The instantaneous heat gain and thermal efficiency can be calculated by:

$$Q_{th} = \dot{m}c_w (T_{out} - T_{in}), \quad (1)$$

$$\eta_{th} = \frac{Q_{th}}{GA_c}, \quad (2)$$

where the  $\dot{m}$  is the mass flow rate of the flowing water measured by the turbine flowmeter (LWGY), kg/s;  $c_w$  is the specific heat capacity of the water, J/kg·K;  $T_{in}$  and  $T_{out}$  are the inlet and outlet temperature of the PV/T collector measured by the Pt resistance (Pt 100), K;  $G$  is the solar radiation measured by the radiometer (TBQ-2), W/m<sup>2</sup>;  $A_c$  is the area of the collector, m<sup>2</sup>.

The electrical gain and efficiency are two important parameters for evaluating the electrical performance, which are given by:

$$P_{pv} = U_{mp} I_{mp}, \quad (3)$$

$$\eta_{pv} = \frac{P_{pv}}{GA_{pv}}, \quad (4)$$

where  $U_{mp}$  is the voltage at the maximum power point, V;  $I_{mp}$  is the current at the maximum power point, A;  $A_{pv}$  is the area of the PV module, m<sup>2</sup>.

The daily average thermal and electrical efficiency are expressed as:

$$\eta_{th,a} = \frac{\sum Q_{th}}{HA_c}, \quad (5)$$

$$\eta_{pv,a} = \frac{\sum P_{pv}}{HA_{pv}}, \quad (6)$$

where  $H$  is daily total radiation, J/m<sup>2</sup>.

To synthesize the effects of ambient temperature, solar radiation, and inlet temperature, and to obtain general conclusions, a linear correlation between thermal efficiency and reduced temperature  $(T_{in}-T_a)/H$  is built, expressed as [29]:

$$\eta_{th,a} = \eta_0 - U_{loss} \frac{T_{in} - \overline{T_{air}}}{H}, \quad (7)$$

where  $\eta_0$  is the daily average thermal efficiency at zero reduced temperature;  $U_{loss}$  represents the amount of heat loss, MJ/m<sup>2</sup>·K;  $\overline{T_{air}}$  is the daily average temperature of the ambient temperature, K.

The calculation of overall energy efficiency takes into account the difference in the energy grade of electricity and heat. The overall energy efficiency is calculated by [30]:

$$\eta_{pvt,a} = \eta_{th,a} + \zeta \frac{\eta_{pv,a}}{\eta_{power}}, \quad (8)$$

where  $\zeta = A_{pv}/A_c$  is the covering factor, and  $\eta_{power}=38\%$  is the electrical efficiency from the traditional heat-engine plant.

The fill factor (FF) is an important parameter for evaluating the output characteristics of PV cells. It is defined as the ratio of the maximum power to the product of short-circuit current and open-circuit voltage. The *FF* is given by:

$$FF = \frac{I_{mp} U_{mp}}{I_{sc} U_{oc}}, \quad (9)$$

where the  $U_{oc}$  is the open-circuit voltage, V;  $I_{sc}$  is the short-circuit current, A.

### 2.3.2 Second-law analysis

The exergy content of thermal energy depends on the temperature at which heat is generated, and the electrical energy is pure exergy. The exergy content of thermal energy and electrical energy can be calculated by [31]:

$$\dot{E}x_{th} = Q_{th} \left( 1 - \frac{T_a}{T_m} \right), \quad (10)$$

$$\dot{E}x_{pv} = P_{pv}, \quad (11)$$

where  $T_m$  is the mean thermodynamic temperature, related to the temperature lift from inlet temperature  $T_{in}$  to outlet temperature  $T_{out}$ , K, and expressed as:

$$T_m = \frac{T_{out} - T_{in}}{\ln(T_{out}/T_{in})}. \quad (12)$$

The exergy content of solar radiation incident on the PV/T collector surface is given by [32]:

$$\dot{E}x_G = G \left( 1 - \frac{T_{\text{air}}}{T_{\text{sun}}} \right), \quad (13)$$

where  $T_{\text{sun}} = 5760\text{K}$  is the apparent solar temperature.

The average exergy efficiency of the heat gain and electrical gain, as well as the overall exergy efficiency, are calculated by:

$$\eta_{\text{ex,th}} = \frac{\sum \dot{E}x_{\text{th}}}{\sum \dot{E}x_G A_c}, \quad (14)$$

$$\eta_{\text{ex,pv}} = \frac{\sum \dot{E}x_{\text{pv}}}{\sum \dot{E}x_G A_{\text{pv}}}, \quad (15)$$

$$\eta_{\text{ex,pvt}} = \eta_{\text{ex,th}} + \zeta \eta_{\text{ex,pv}}. \quad (16)$$

### 2.3.3 Thermal resistance analysis

The overall thermal resistance between the working fluid and ambient air  $R_t$  is a useful indicator for the mechanical structure of the two PV/T systems. In the situation of breakdown or fracture, the contact of components will be modified, leading to a change of  $R_t$ . The overall thermal resistance  $R_t$  is calculated by:

$$R_t = 1/h_t, \quad (17)$$

$$\dot{m}c_w (T_{\text{out}} - T_{\text{in}}) = h_t A_t (T_a - T_m), \quad (18)$$

where  $h_t$  is the overall coefficient of heat transfer,  $\text{W}/\text{m}^2 \cdot \text{K}$ ;  $A_t$  is the total external area of the a-Si PV/T collector,  $\text{m}^2$ .

## 3. Results and discussions

Outdoor experiments on the long-term behavior of the a-Si PV/T systems operating at medium temperature ( $60\text{ }^\circ\text{C}$ ) and low temperature ( $30\text{ }^\circ\text{C}$ ) have been carried out from December 2017 to June

2019. The experimental results from 10:00 to 15:00 of 56 sunny or cloudy days are summarized and given. The daily average ambient temperature and total solar radiation are shown in Fig. 6. The red line represents the variation of the daily average ambient temperature, which is higher in summer and lower in winter. The maximum and minimum daily average ambient temperatures are 36.9 °C and 2.6 °C, and the daily total solar radiation varies from 9.53 MJ/m<sup>2</sup> to 16.91 MJ/m<sup>2</sup>.

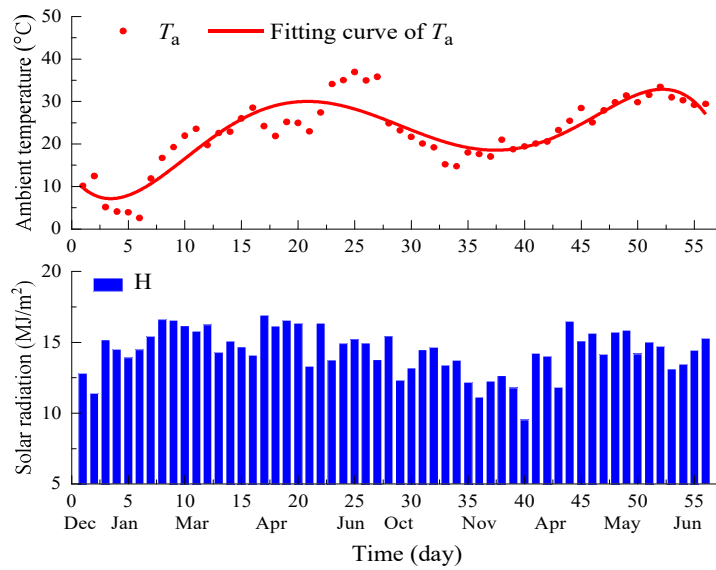


Fig. 6. Daily average ambient temperature and total solar radiation.

### 3.1 Daily energetic performance

#### 3.1.1 Heat collection

The thermal performances of the a-Si PV/T systems operating at 30 °C and 60 °C are compared in Fig. 7. The detailed multi-day results of the two systems at the operating temperature of 30 °C and 60 °C are also shown in Appendix 1. The thermal efficiency of the a-Si PV/T system operating at 60 °C is significantly lower than that at 30 °C, since the higher operating temperature leads to a greater heat loss. It is observed that the thermal efficiency is related to the ambient temperature and mass flow rate. A higher ambient temperature means a lower heat loss between the collector and surrounding air and

enables a higher thermal efficiency. The heat transfer between the copper tube and flowing water is enhanced with a larger mass flow rate, resulting in an increased thermal efficiency.

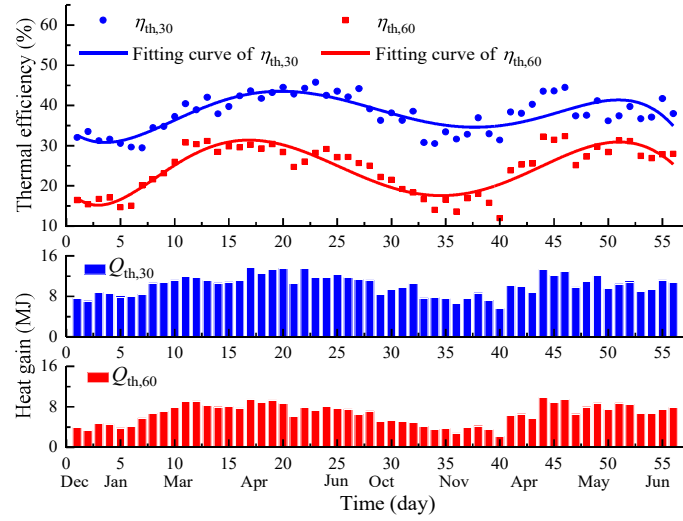


Fig. 7. Thermal performance of the a-Si PV/T systems at 30 °C and 60 °C.

A linear fitting curve of the daily average thermal efficiency against  $(T_{in}-\bar{T}_a)/H$  at 30 °C and 60 °C, as shown in Fig. 8. The thermal efficiency can be expressed as a regression formula:

$$\eta_{th,a,30} = 0.4125 - 6.21 \frac{T_{in} - \bar{T}_a}{H}, \quad (19)$$

$$\eta_{th,a,60} = 0.4287 - 7.08 \frac{T_{in} - \bar{T}_a}{H}. \quad (20)$$

The regression lines and equations of thermal efficiency operating at 30 °C and 60 °C suggest that the intercept daily average thermal efficiencies are 41.25% and 42.87% respectively when the inlet temperature is equal to the ambient temperature. With the increase of  $(T_{in}-\bar{T}_a)/H$ , the daily average thermal efficiency decreases gradually and the slope is  $-6.21$  and  $-7.08$  for 30 °C and 60 °C. Because these two a-Si PV/T systems make no odds, the intercept  $\eta_0$  and the slope  $U_{loss}$  are supposed to be independent on the operating temperature. However, part of solar energy received by the PV/T collector is converted into heat rather than electricity through the PV cell, and the excess heat is

recovered by the working fluid. The electrical efficiency at 60 °C is slightly lower than that at 30 °C (see Section 3.1.2), so the power conversion at different temperatures has a minor influence on the thermal efficiency. Moreover, Eqs. (19) and (20) are the first order of approximation of the collector thermal efficiency. The efficiency of a collector is expected to drop more significantly at a higher operating temperature. Since the value of the slope  $U_{\text{loss}}$  represents the first heat loss coefficient of the collector and the heat loss increases parabolically with the operating temperature, the slope of the efficiency curve at 60 °C is higher than that at 30 °C, leading to a slightly higher intercept efficiency at 60 °C.

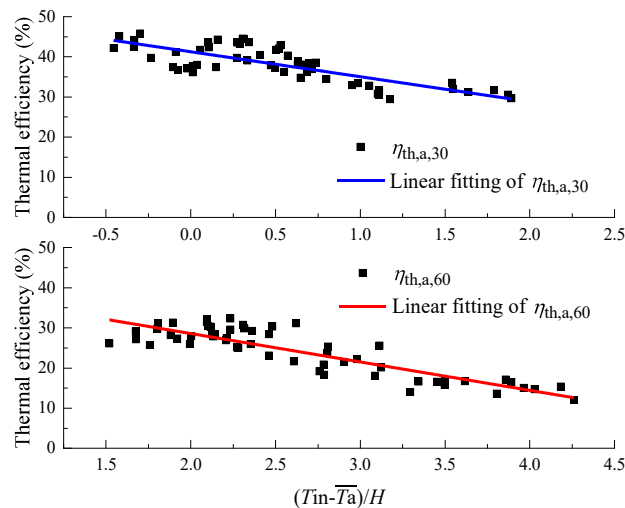


Fig. 8. Linear fitting of daily average thermal efficiency of a-Si PV/T collector at 30 °C and 60 °C.

### 3.1.2 Power generation

The long-term experimental results of the electrical performance at 30 °C and 60 °C are shown in Fig. 9 and the detailed multi-day results of electrical performance are displayed in Appendix 1. It is intuitively observed that the operating temperature plays an important role in the electrical performance of a-Si cells. The electrical efficiencies at 30 °C and 60 °C are both declined with time, which is caused by the S-W effect related to the light-induced degradation and the creation of defect

1 states. However, the difference in electrical efficiency between 30 °C and 60 °C is gradually narrowing.  
2  
3 When the inlet water temperature is 60 °C, the daily average electrical efficiency is highest at 5.69%  
4  
5 on December 25, 2017, while it reduces to 5.32% on June 23, 2019 during the long-term operation.  
6  
7 For the inlet water temperature of 30 °C, the electrical efficiency on December 25, 2017, and June 23,  
8  
9 2019 is 6.15% and 5.45%, respectively. The difference in the electrical efficiency between 30 °C and  
10  
11 60 °C is 0.47% at the beginning. After the long-term light-induced degradation, the gap narrows to  
12  
13 only 0.13%. As a comparison, for a conventional PV/T system using c-Si cells and having an efficiency  
14  
15 of 12% at the standard test condition, the temperature coefficient is about  $-0.5 \text{ \%/}^\circ\text{C}$  and the difference  
16  
17 in the electrical efficiency between 30 °C and 60 °C of the c-Si PV/T can be 1.8%, which is  
18  
19 significantly higher than that of the a-Si PV/T (0.13%). Besides, a-Si cells exhibit higher electrical  
20  
21 efficiency in summer but lower electrical efficiency in winter [33, 34], which can also be revealed  
22  
23 from Fig. 9. For example, the values in January, March, and November (No.5-12 and No.33-40) are  
24  
25 generally below the fitting curve, while they are mostly above the fitting curve in April, May, and June  
26  
27 (No. 13-32 and No. 41-50). The variation of the normalized electrical performance is displayed in Fig.  
28  
29 10, and the result is consistent with that found by Rozario et al.[13]. The electrical efficiencies of a-Si  
30  
31 cells degrade by 11.5% and 6.5% at 30 °C and 60 °C, respectively.  
32  
33  
34  
35  
36  
37  
38  
39  
40  
41  
42  
43  
44

45 The performance of a-Si cells is undermined because long-time light exposure reduces the electrical  
46  
47 efficiency. Fortunately, the results of this study show that a-Si cells have the ability to reduce the  
48  
49 degradation at high temperatures. This characteristic confirms the advantages of the a-Si cells in the  
50  
51 medium-high temperature PV/T application where the operating temperature can reach 60-100 °C.  
52  
53  
54  
55  
56  
57  
58  
59  
60  
61  
62  
63  
64  
65

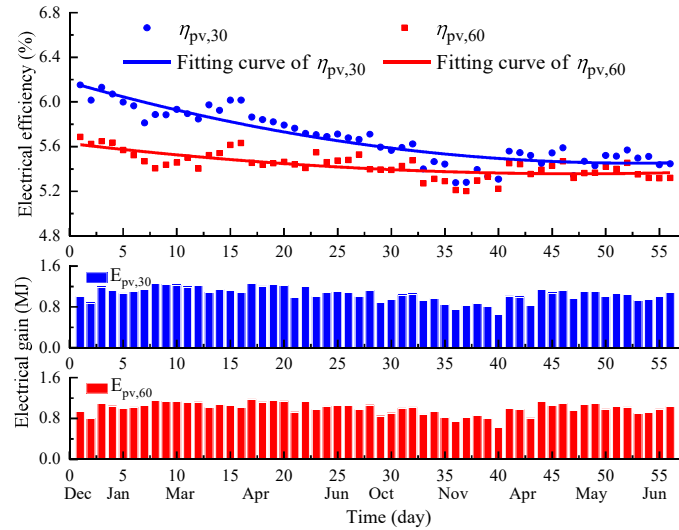


Fig. 9. Electrical performance of the a-Si PV/T systems at 30 °C and 60 °C.

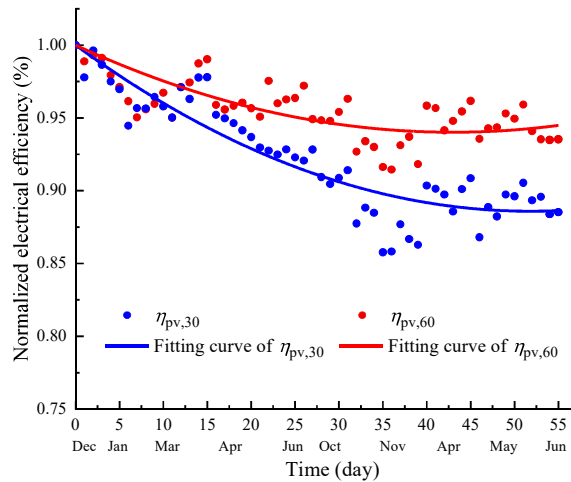


Fig. 10. The normalized electrical efficiency of the a-Si PV/T systems at 30 °C and 60 °C.

### 3.1.3 Overall performance

The overall energy efficiency takes into account the difference in the energy grade of electricity and heat. As shown in Fig. 11, the variation of overall energy efficiency is quite similar to that of the daily thermal efficiency. The overall energy efficiency at 30 °C ranges from 39.99% to 56.10%, whilst it is in the range of 21.43% - 42.27% at 60 °C.

During the prolonged operation from December 2017 to June 2019, the two a-Si PV/T systems have

operated reliably without significant degradation in thermal and electrical performance (except for the light-induced degradation of a-Si cells).

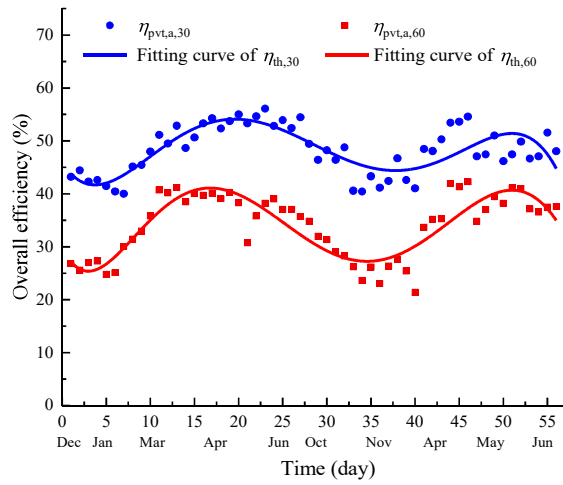


Fig. 11. Overall energy efficiency of the a-Si PV/T systems at 30 °C and 60 °C.

### 3.2. Daily exergetic performance

The previous analyses are based on the first law of thermodynamics and do not take into account the different qualities of heat and power produced by the a-Si PV/T collectors. The thermal and electrical exergy are especially relevant in PV/T systems, where the useful energy output capability is greatly affected by the operating temperature [35]. Compared to a simple energy analysis, the exergy analysis can provide a broader perspective. For this purpose, the exergy analysis of the long-term performance of a-Si PV/T systems at different operating temperatures is performed in this section. The detailed results of exergy performance at 30 °C and 60 °C are displayed in Appendix 2.

The exergy efficiency regarding electricity gain of the a-Si PV/T systems at 30 °C and 60 °C is shown in Fig. 12. Here, one can observe the same trend as the electrical efficiency (see Fig. 9). This exergetic efficiency as defined by Eq. (15) is slightly higher than the electrical efficiency, since the exergy content of solar radiation  $\dot{E}x_G$  is lower than the solar radiation  $G$ . The difference in the electricity-based exergy efficiency between 30 °C and 60 °C decreases from 0.49% to 0.14%

throughout the prolonged operation.

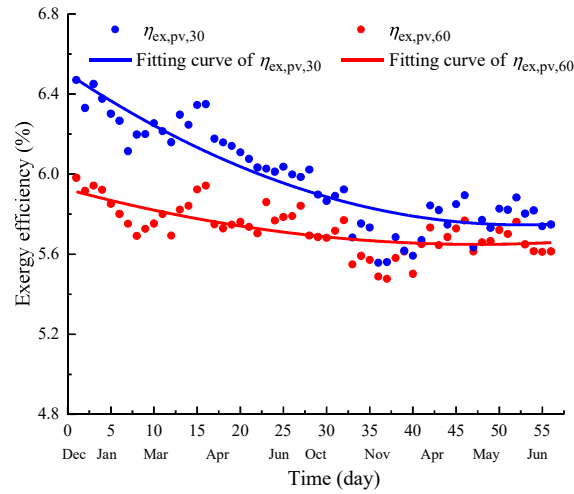


Fig. 12. Exergy efficiency regarding electricity gain of the a-Si PV/T systems at 30 °C and 60 °C.

Aside from electricity, heat is the useful energy of the PV/T system. The exergy efficiency regarding the heat gain and the overall exergy efficiency are depicted in Fig. 13. The results show that the heat-based exergy efficiency at 30 °C and 60 °C have an opposite variation tendency to the thermal efficiency (see Fig. 7). The heat-based exergy efficiency and overall exergy efficiency at 30 °C are generally lower than those at 60 °C. Particularly, there is an obvious difference in exergy efficiency at 30 °C and 60 °C from March to June. The thermal efficiency indicates the amount of energy which is utilized regardless of its quality. Although the thermal efficiency in low-temperature operation is higher, the exergy efficiency can be lower since heat is less useful if the operating temperature is close to the ambient temperature.

With the operating temperature of 60 °C, higher exergy efficiencies for the thermal energy appear in March and April, when the ambient temperature is around 20-25 °C. In other months, the exergy efficiency shows a lower level, especially in October, November, and December. The exergy efficiency at 30 °C is the lowest in June when the daily average ambient temperature is the highest during the test; on the contrary, a higher efficiency is achieved in winter (October, November, and December).

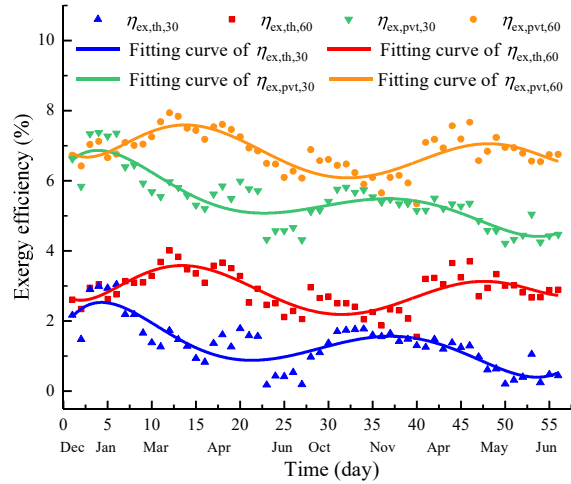
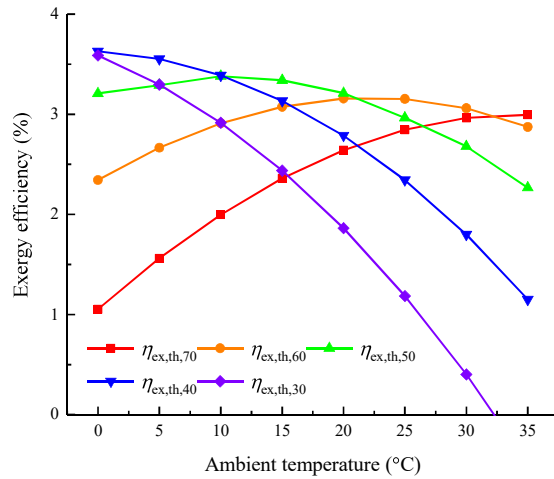


Fig. 13. Exergy efficiency regarding the heat gain and overall exergy efficiency of the a-Si PV/T systems at 30 °C and 60 °C.

As previously discussed, the month for the highest exergy efficiency at 30 °C differs from that at 60 °C, which is largely dependent on the ambient temperature. To investigate the exergy efficiency regarding the heat gain of the a-Si PV/T system at different ambient temperatures and inlet temperatures, a simulation is carried out based on an experimentally validated model [8]. The simulation is under the following assumptions: solar radiation of 800 W/m<sup>2</sup> and mass flow rate of 0.04 kg/s and the structure parameters of the model are the same as those of the actual PV/T collector. The exergy efficiency is a trade-off between the amount of heat gain and its quality. Given the operating temperature, a lower ambient temperature leads to less heat gain but better quality. As shown in Fig. 14, when the inlet temperatures are 30 °C and 40 °C, the exergy efficiency decreases as the ambient temperature rises from 0 °C to 35 °C. Conversely, when the inlet temperature is 70 °C, it exhibits an upward trend with increasing ambient temperature. There is a maximum exergy efficiency at inlet temperatures of 50 °C and 60 °C. When the inlet temperature is 60 °C, the maximum exergy efficiency occurs at the ambient temperature around 20 °C to 25 °C, which is identical with the experimental

1 results. In addition, when the ambient temperature is higher than 10 °C, the exergy efficiency at 60 °C  
 2 is greater than that at 30 °C. This is consistent with the fact that the exergy efficiency at 30 °C is higher  
 3 than that at 60 °C only in January (No.3- No.6).  
 4  
 5  
 6  
 7

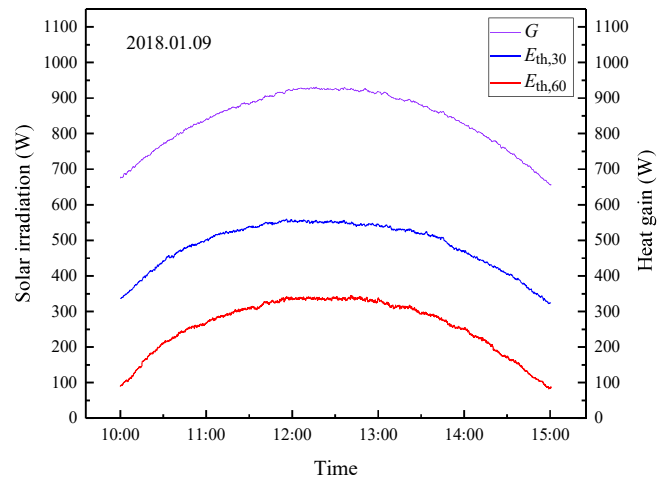


8  
 9  
 10  
 11  
 12  
 13  
 14  
 15  
 16  
 17  
 18  
 19  
 20  
 21  
 22  
 23  
 24  
 25 Fig. 14. Simulation results of the exergy efficiency regarding the heat gain at different ambient  
 26 temperatures and inlet temperatures.  
 27

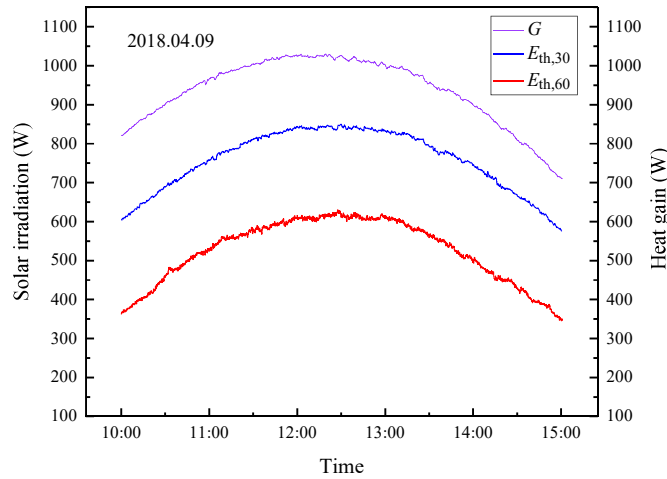
### 28 3.3. Detailed comparison in the early, middle and late stages of the test

29  
 30 The detailed performances of the a-Si PV/T systems at 30 °C and 60 °C for three typical days  
 31 (January 9, 2018, April 9, 2018, and June 23, 2019) are presented in this section. January 9, 2018 and  
 32 June 23, 2019 represent the thermal and electrical performance at the initial and final phases of the  
 33 long-term experiments respectively. Although there are only three months from the initial phase, April  
 34 9, 2018 can represent the intermediate phase because the performance of a-Si cells normally degrades  
 35 fast in the first 6 months [36]. For these three days, the daily average ambient temperatures are 5.3 °C,  
 36 24.2 °C and 29.4 °C, and the daily total solar radiations are 15.17 MJ/m<sup>2</sup>, 16.91 MJ/m<sup>2</sup> and 15.27  
 37 MJ/m<sup>2</sup>. As shown in Fig. 15, the variation of the heat gain is identical with the solar radiation. For the  
 38 a-Si PV/T system operating at 30 °C, the total heat gains on January 9<sup>th</sup>, April 9<sup>th</sup>, and June 23<sup>rd</sup> are  
 39 8.77 MJ, 13.68 MJ, and 10.74 MJ, with the daily average thermal efficiency of 31.22%, 43.66%, and  
 40  
 41  
 42  
 43  
 44  
 45  
 46  
 47  
 48  
 49  
 50  
 51  
 52  
 53  
 54  
 55  
 56  
 57  
 58  
 59  
 60  
 61  
 62  
 63  
 64  
 65

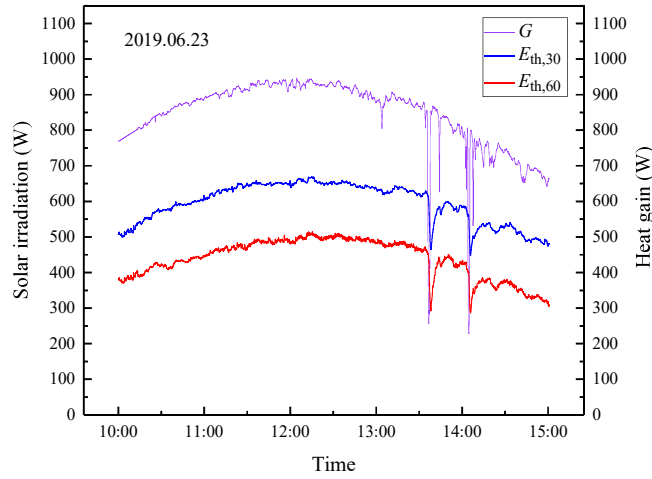
37.98%, respectively. When the inlet water temperature is 60 °C, the total heat gains are 4.70 MJ, 9.48 MJ, and 7.92 MJ respectively, and the average thermal efficiencies are 16.74%, 30.25%, and 27.99%. The variations of electrical performance at 30 °C and 60 °C on January 9<sup>th</sup>, April 9<sup>th</sup>, and June 23<sup>rd</sup> are shown in Fig. 16. It is observed that the difference in the electrical efficiency between 30 °C and 60 °C is gradually reduced. The daily average electrical efficiencies at 30 °C are 6.13%, 5.86%, and 5.45%, meanwhile at 60 °C are 5.65%, 5.45%, and 5.32%.



(a)

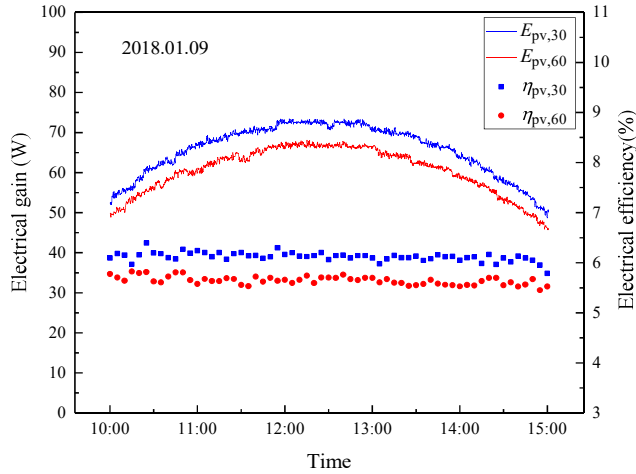


(b)

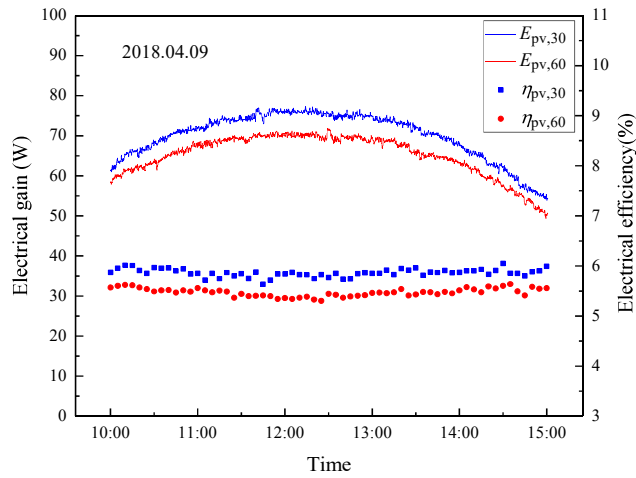


(c)

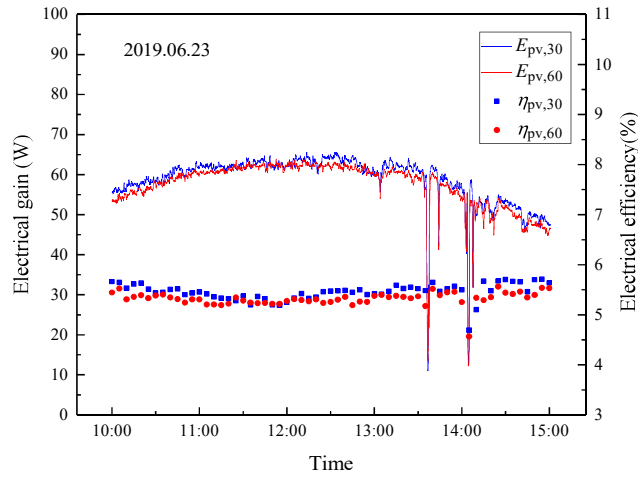
Fig. 15. Variations of solar radiation and heat gain at 30 °C and 60 °C on January 9, 2018, April 9, 2018, June 23, 2019.



(a)



(b)



(c)

Fig. 16. Variations of electrical performance at 30 °C and 60 °C on January 9, 2018, April 9, 2018, June 23, 2019.

The I-V characteristics curves of the a-Si PV/T systems with the solar radiation of about 900W/m<sup>2</sup> on the three chosen days are shown in Fig. 17. The detailed results of the I-V characteristics at 30 °C and 60 °C, such as solar radiation, open-circuit voltage, short-circuit current, maximum power point voltage and current, and FF, are all given in Table 1. When the inlet water temperature is 30 °C, the FFs are 57.95%, 56.91% and 52.05% on January 9<sup>th</sup>, April 9<sup>th</sup>, and June 23<sup>rd</sup>, whilst they are 57.33%, 56.74% and 52.16% with the inlet water temperature of 60 °C. The FFs at 30 °C and 60 °C are both on the decline, but the difference in FFs between the two operating temperatures is minimal.

1  
2  
3  
4  
5  
6  
7  
8  
9  
10  
11  
12  
13  
14  
15  
16  
17  
18  
19  
20  
21  
22  
23  
24  
25  
26  
27  
28  
29  
30  
31  
32  
33  
34  
35  
36  
37  
38  
39  
40  
41  
42  
43  
44  
45  
46  
47  
48  
49  
50  
51  
52  
53  
54  
55  
56  
57  
58  
59  
60  
61  
62  
63  
64  
65

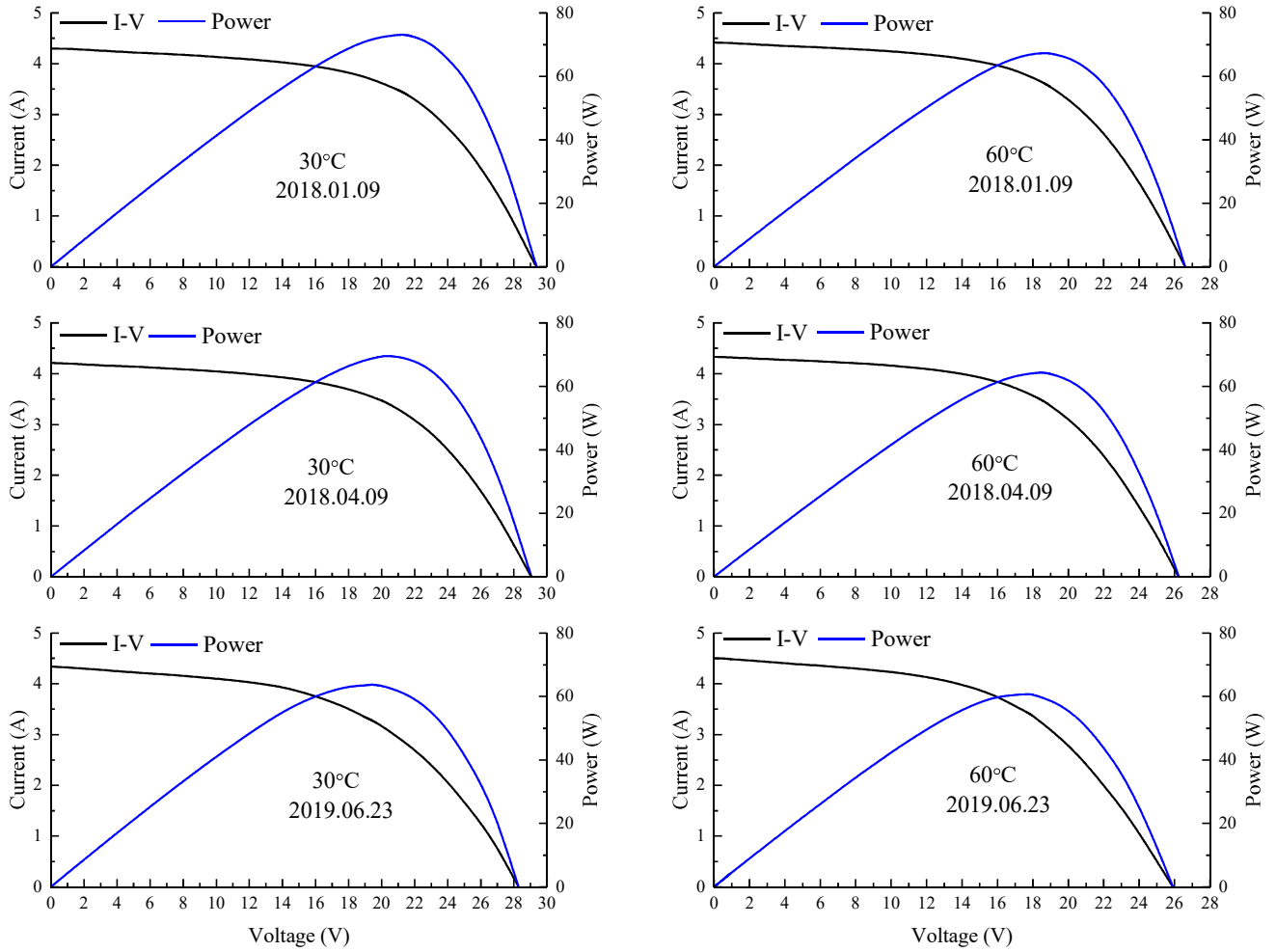


Fig. 17. I-V characteristics curve of the a-Si PV/T systems operating at 30 °C and 60 °C.

Table 1 Detailed results of I-V characteristics at temperatures 30 °C and 60 °C.

Date	$T_{in}$ (°C)	$G$ (W/m <sup>2</sup> )	$U_{oc}$ (V)	$I_{sc}$ (A)	$U_{mp}$ (V)	$I_{mp}$ (A)	$P_{mp}$ (W)	$\eta_{pv}$ (%)	$FF$ (%)
2018.01.09	30	922.6	29.38	4.30	21.37	3.43	73.21	6.22	57.95
	60	924.4	26.59	4.42	18.73	3.60	67.38	5.71	57.33
2018.04.09	30	909.3	29.05	4.21	20.16	3.45	69.60	6.00	56.91
	60	907.3	26.23	4.33	18.58	3.47	64.45	5.57	56.75
2019.06.23	30	916.6	28.21	4.34	19.37	3.29	63.72	5.45	52.05
	60	910.5	25.90	4.50	17.80	3.42	60.79	5.23	52.16

### 3.4 Mechanical fault detection

It is important to estimate the temperature influence on the mechanical structure. With a damaged structure, the lifetime of the PV/T system will be shortened. For PV/T systems using c-Si cells,

1 mechanical fault and breakdown due to the thermal stress at periodic fluctuating temperature have  
2 been reported [21]. This problem may be eased for a-Si PV/T systems in regard to the thin-film  
3 characteristic of the cells. As shown in Fig. 18, there is no significant difference in appearance between  
4 the two prototypes at the end of the long-term test.  
5  
6  
7  
8  
9



10  
11  
12  
13  
14  
15  
16  
17  
18  
19  
20  
21  
22  
23  
24  
25  
26  
27  
28  
29  
30  
31  
32 Fig. 18. External images of the two a-Si PV/T collectors.  
33  
34

35 Since the prototypes are in operation, an insight of the structure is not available. It is difficult to  
36 directly detect the inner mechanical faults. However, in any situation of abrupt and deformation,  
37 the thermodynamic properties of the PV/T systems will be affected. The a-Si cells are deposited on the  
38 stainless steel and the latter is laminated on the aluminum absorber. The interface between the substrate  
39 and absorber is correlated with the mechanical combination. Thermal contact resistance is an  
40 alternative indicator for indirect mechanical fault detection. The overall thermal resistance between  
41 water and ambient air will vary as the contact resistance changes.  
42  
43  
44  
45  
46  
47  
48  
49  
50  
51  
52  
53

54 To compare the overall thermal resistance of the two prototypes after the long-term operation,  
55 experimental tests were conducted under the same boundary conditions. The inlet water temperatures  
56  
57  
58  
59  
60  
61  
62  
63  
64  
65

of the PV/T collectors were both controlled to be 45 °C with a mass flow rate of 0.03kg/s. The variations of the ambient temperature, glass cover temperature, and absorber plate temperature are displayed in Fig. 19. The temperatures of the glass cover and absorber plate have no appreciable difference between the two PV/T systems. The variations of the overall thermal resistance and the temperature difference between the outlet and inlet are depicted in Fig. 20. The average thermal resistances during the test each are 0.618 m<sup>2</sup>·K/W and 0.621 m<sup>2</sup>·K/W. There is a negligible difference in the overall thermal resistance of the two a-Si PV/T collectors. It confirms that the temperature has no significant effect on the mechanical structure over an almost two-year operation and there is no technical failure and observable deformation in these two a-Si PV/T collectors at 30 °C and 60 °C.

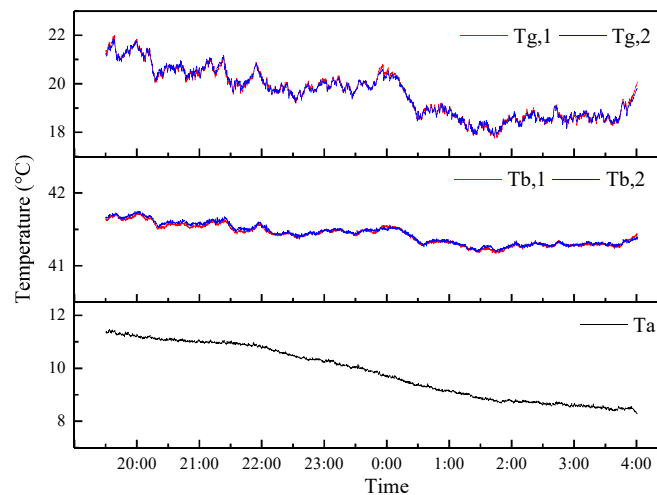


Fig. 19. Variations of the ambient temperature, glass cover temperature and absorber plate temperature with time at 45°C.

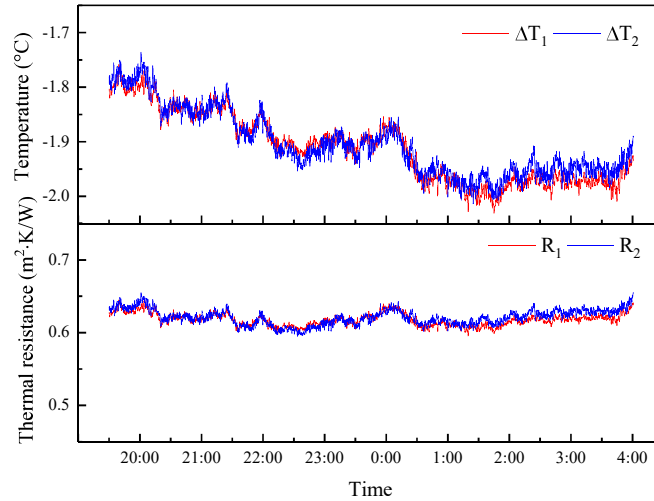


Fig. 20. Variations of the overall thermal resistance and the temperature difference with time at 45°C.

## 6. Conclusions

Operating temperature has a crucial impact on the thermal, electrical and mechanical performance of the a-Si PV/T system. In this paper, the temperature-dependent performance of the a-Si PV/T system has been explored by the long-term outdoor experiments in the natural environment from December 2017 to June 2019. Two identical a-Si PV/T systems have been tested at a low temperature of 30 °C and a medium temperature of 60 °C.

Results show that the intercept daily average thermal efficiency is 41.25% for 30 °C and 42.87% for 60 °C. As the normalized temperature difference increases, the daily average thermal efficiencies decrease with a slope of  $-6.21$  and  $-7.08$ .

The initial electrical efficiencies of the two a-Si PV/T systems at 30 °C and 60 °C are 6.15% and 5.69%, respectively. In the initial stage, the difference in the electrical efficiency of a-Si cells between 30 °C and 60 °C is 0.47%, and after a long-term outdoor operation, the gap narrows to only 0.13%, which is inappreciable compared to the efficiency variation of conventional PV/T systems using c-Si cells. The electrical properties of a-Si cells degrade by 11.5% and 6.5% at 30 °C and 60 °C. This

characteristic makes a-Si cells suitable in the PV/T application.

The exergetic analysis shows that the exergy efficiency at 30 °C and 60 °C has the opposite changing trend to the thermal efficiency. The heat-based exergy efficiency and overall exergy efficiency at 60 °C are significantly higher than those at 30 °C, which further demonstrates the advantage of the a-Si PV/T operating at medium temperature.

During the long-term operation, the two a-Si PV/T systems can operate stably without significant degradation in thermal and electrical performance. Moreover, there is no detectable technical failure and observable deformation appeared in these two a-Si PV/T systems.

## Acknowledgments

This study was sponsored by the National Science Foundation of China (NSFC 51776193, and 51761145109).

## Appendix 1. Performance comparison of a-Si PV/T systems at 30 °C and 60 °C.

No	Date	$\bar{T}_a$ (°C)	$H$ (MJ/m <sup>2</sup> )	$\dot{m}$ (kg/s)		$Q_{th}$ (MJ)		$\eta_{th,a}$ (%)		$P_{pv}$ (MJ)		$\eta_{pv,a}$ (%)		$\eta_{pvt,a}$ (%)	
				30	60	30	60	30	60	30	60	30	60	30	60
1	2017.12.25	10.2	12.80	0.041	0.036	7.60	3.91	32.05	16.47	1.01	0.93	6.15	5.69	43.20	26.78
2	2017.12.26	12.5	11.37	0.036	0.036	7.06	3.24	33.54	15.38	0.87	0.80	6.02	5.62	44.45	25.58
3	2018.01.09	5.3	15.17	0.040	0.036	8.77	4.70	31.22	16.74	1.18	1.09	6.13	5.65	42.34	26.98
4	2018.01.10	4.1	14.49	0.044	0.044	8.49	4.59	31.63	17.08	1.12	1.04	6.07	5.64	42.63	27.30
5	2018.01.11	3.9	13.92	0.031	0.028	7.89	3.79	30.59	14.69	1.07	0.99	6.00	5.57	41.46	24.79
6	2018.01.12	2.6	14.48	0.030	0.036	7.95	4.04	29.64	15.08	1.10	1.02	5.97	5.52	40.45	25.09
7	2018.03.09	11.9	15.41	0.024	0.028	8.41	5.75	29.46	20.15	1.14	1.08	5.81	5.47	39.99	30.06
8	2018.03.10	16.7	16.60	0.031	0.026	10.61	6.65	34.51	21.63	1.24	1.15	5.89	5.41	45.18	31.43
9	2018.03.11	19.3	16.56	0.028	0.028	10.67	7.09	34.78	23.12	1.24	1.15	5.89	5.44	45.45	32.98
10	2018.03.12	22.0	16.17	0.030	0.026	11.16	7.77	37.24	25.93	1.22	1.13	5.93	5.46	48.00	35.82
11	2018.03.13	23.6	15.79	0.038	0.042	11.83	9.00	40.44	30.77	1.19	1.11	5.89	5.50	51.13	40.75
12	2018.03.23	19.7	16.23	0.036	0.042	11.71	9.13	38.93	30.36	1.21	1.12	5.85	5.40	49.53	40.16
13	2018.03.26	22.6	14.27	0.039	0.043	11.11	8.24	42.03	31.16	1.09	1.01	5.97	5.52	52.86	41.17
14	2018.03.27	22.9	15.08	0.028	0.031	10.60	7.95	37.92	28.45	1.14	1.07	5.92	5.54	48.67	38.49
15	2018.03.31	26.0	14.67	0.028	0.031	10.80	8.11	39.72	29.85	1.13	1.05	6.02	5.62	50.63	40.03

16	2018.04.02	28.5	14.09	0.028	0.031	11.07	7.71	42.39	29.54	1.08	1.01	6.02	5.63	53.30	39.75
17	2018.04.09	24.2	16.91	0.029	0.039	13.70	9.48	43.73	30.25	1.26	1.18	5.86	5.45	54.28	40.14
18	2018.04.17	21.9	16.14	0.028	0.031	12.48	8.75	41.74	29.26	1.20	1.12	5.84	5.44	52.33	39.11
19	2018.04.18	25.2	16.56	0.028	0.033	13.25	9.33	43.20	30.40	1.23	1.15	5.82	5.45	53.75	40.28
20	2018.05.09	25.0	16.36	0.029	0.031	13.49	8.61	44.53	28.42	1.21	1.14	5.79	5.46	55.03	38.32
21	2018.05.10	23.0	13.31	0.028	0.028	10.57	5.15	42.85	20.89	0.98	0.92	5.76	5.44	53.30	30.75
22	2018.06.06	26.3	16.35	0.028	0.026	13.41	7.88	44.29	26.01	1.19	1.13	5.72	5.41	54.66	35.81
23	2018.06.07	34.1	13.76	0.024	0.028	11.67	7.19	45.76	28.20	1.00	0.97	5.71	5.55	56.10	38.26
24	2018.06.11	35.0	14.91	0.023	0.026	11.74	8.05	42.51	29.15	1.08	1.04	5.69	5.46	52.83	39.05
25	2018.06.12	36.9	15.19	0.023	0.023	12.26	7.63	43.56	27.13	1.11	1.06	5.71	5.47	53.91	37.06
26	2018.06.13	35.0	14.94	0.024	0.023	12.87	7.52	42.14	27.17	1.08	1.04	5.68	5.48	52.44	37.11
27	2018.06.15	35.8	13.77	0.024	0.023	11.96	6.55	44.19	25.69	1.00	0.97	5.66	5.53	54.46	35.71
28	2018.10.29	24.9	15.41	0.033	0.031	11.17	7.14	39.11	25.02	1.12	1.06	5.71	5.40	49.47	34.81
29	2018.10.30	23.2	12.34	0.031	0.031	8.29	5.07	36.27	22.19	0.88	0.85	5.59	5.39	46.42	31.97
30	2018.10.31	21.7	13.20	0.033	0.031	9.33	5.26	38.17	21.53	0.93	0.91	5.55	5.39	48.26	31.30
31	2018.11.01	20.1	14.46	0.034	0.028	9.72	5.15	36.30	19.22	1.03	1.00	5.59	5.43	46.43	29.06
32	2018.11.02	19.2	14.64	0.036	0.034	10.46	4.97	38.56	18.34	1.05	1.02	5.62	5.48	48.75	28.27
33	2018.11.22	15.2	13.39	0.027	0.029	7.64	4.14	30.79	16.67	0.92	0.90	5.40	5.27	40.58	26.22
34	2018.11.23	14.8	13.72	0.028	0.026	7.76	3.57	30.52	14.04	0.96	0.93	5.47	5.31	40.43	23.67
35	2018.11.24	18.0	12.17	0.028	0.028	7.54	3.74	33.43	16.58	0.84	0.82	5.44	5.29	43.30	26.17
36	2018.11.25	17.7	11.13	0.028	0.026	6.52	2.81	31.62	13.61	0.75	0.74	5.28	5.21	41.18	23.06
37	2018.11.26	17.2	12.27	0.028	0.029	7.46	3.85	32.84	16.94	0.83	0.81	5.28	5.20	42.41	26.37
38	2018.11.27	21.0	12.64	0.029	0.029	8.64	4.23	36.92	18.09	0.87	0.85	5.39	5.30	46.70	27.69
39	2018.11.28	18.8	11.79	0.028	0.029	7.20	3.45	32.95	15.77	0.80	0.80	5.33	5.33	42.62	25.44
40	2018.11.29	19.4	9.53	0.028	0.029	5.54	2.11	31.40	12.07	0.65	0.63	5.31	5.22	41.03	21.43
41	2019.04.12	20.1	14.22	0.039	0.035	10.11	6.28	38.39	23.83	1.01	0.99	5.56	5.45	48.47	33.71
42	2019.04.15	20.6	14.02	0.039	0.039	9.88	6.57	38.04	25.31	0.99	0.97	5.55	5.44	48.09	35.18
43	2019.04.16	23.3	11.80	0.040	0.043	8.81	5.59	40.28	25.58	0.83	0.81	5.52	5.35	50.29	35.29
44	2019.04.17	25.5	16.48	0.042	0.043	13.30	9.83	43.56	32.20	1.15	1.13	5.45	5.39	53.43	41.98
45	2019.04.18	28.4	15.17	0.042	0.042	12.17	8.79	43.59	31.48	1.07	1.04	5.54	5.43	53.64	41.32
46	2019.04.19	25.1	15.62	0.041	0.043	12.87	9.36	44.46	32.35	1.11	1.09	5.59	5.47	54.59	42.27
47	2019.05.21	27.9	14.13	0.031	0.031	9.79	6.58	37.42	25.16	0.96	0.95	5.34	5.32	47.10	34.80
48	2019.05.22	29.8	15.71	0.031	0.031	10.93	7.95	37.54	27.31	1.10	1.08	5.47	5.36	47.46	37.03
49	2019.05.23	31.4	15.85	0.034	0.034	12.09	8.73	41.19	29.74	1.10	1.09	5.43	5.37	51.03	39.47
50	2019.06.02	29.8	14.18	0.031	0.032	9.50	7.47	36.16	28.44	1.00	0.98	5.52	5.42	46.17	38.26
51	2019.06.03	31.6	15.01	0.029	0.032	10.41	8.71	37.44	31.30	1.06	1.03	5.51	5.40	47.44	41.09
52	2019.06.04	33.5	14.70	0.031	0.031	10.82	8.47	39.74	31.12	1.04	1.02	5.57	5.45	49.84	41.01
53	2019.06.11	31.0	13.12	0.034	0.031	8.92	6.67	36.71	27.44	0.92	0.90	5.50	5.35	46.68	37.14
54	2019.06.12	30.3	13.45	0.031	0.031	9.24	6.70	37.11	26.91	0.94	0.91	5.51	5.32	47.10	36.55
55	2019.06.14	29.2	14.44	0.032	0.029	11.15	7.45	41.71	27.87	1.00	0.98	5.44	5.32	51.57	37.51
56	2019.06.23	29.4	15.27	0.028	0.028	10.74	7.92	37.98	27.99	1.06	1.04	5.45	5.32	48.04	37.64

## Appendix 2. Exergy performance comparison of a-Si PV/T systems at 30 °C and 60 °C.

No	Date	$\eta_{ex,th}$ (%)		$\eta_{ex,pv}$ (%)		$\eta_{ex,pvt}$ (%)		No	Date	$\eta_{ex,th}$ (%)		$\eta_{ex,pv}$ (%)		$\eta_{ex,pvt}$ (%)	
		30	60	30	60	30	60			30	60	30	60	30	60
1	2017.12.25	2.17	2.61	6.47	5.98	6.62	6.73	29	2018.10.30	1.10	2.66	5.90	5.69	5.16	6.57
2	2017.12.26	1.48	2.34	6.33	5.92	5.84	6.42	30	2018.10.31	1.37	2.70	5.87	5.68	5.41	6.61

3	2018.01.09	2.90	2.94	6.45	5.94	7.34	7.04	31	2018.11.01	1.70	2.50	5.89	5.72	5.76	6.44
4	2018.01.10	2.99	3.04	6.38	5.92	7.38	7.12	32	2018.11.02	1.73	2.50	5.92	5.77	5.82	6.48
5	2018.01.11	2.93	2.62	6.30	5.85	7.27	6.66	33	2018.11.22	1.76	2.41	5.68	5.55	5.67	6.23
6	2018.01.12	3.04	2.76	6.27	5.80	7.36	6.76	34	2018.11.23	1.77	2.05	5.75	5.59	5.74	5.90
7	2018.03.09	2.19	3.13	6.11	5.75	6.40	7.10	35	2018.11.24	1.59	2.25	5.73	5.57	5.54	6.09
8	2018.03.10	2.18	3.08	6.20	5.69	6.45	7.01	36	2018.11.25	1.56	1.87	5.56	5.49	5.39	5.65
9	2018.03.11	1.66	3.10	6.20	5.73	5.93	7.04	37	2018.11.26	1.64	2.33	5.56	5.48	5.47	6.09
10	2018.03.12	3.18	3.29	6.25	5.75	5.69	7.25	38	2018.11.27	1.42	2.31	5.69	5.58	5.34	6.15
11	2018.03.13	1.27	3.69	6.21	5.80	5.55	7.68	39	2018.11.28	1.48	2.07	5.62	5.61	5.35	5.93
12	2018.03.23	1.73	4.01	6.16	5.69	5.97	7.94	40	2018.11.29	1.30	1.55	5.59	5.50	5.15	5.34
13	2018.03.26	1.47	3.83	6.30	5.82	5.81	7.84	41	2019.04.12	1.25	3.20	5.67	5.65	5.16	7.09
14	2018.03.27	1.28	3.47	6.25	5.84	5.58	7.50	42	2019.04.15	1.47	3.23	5.84	5.73	5.50	7.18
15	2018.03.31	0.93	3.35	6.34	5.92	5.30	7.44	43	2019.04.16	1.20	3.05	5.82	5.64	5.20	6.94
16	2018.04.02	0.83	3.09	6.35	5.94	5.20	7.18	44	2019.04.17	1.38	3.65	5.75	5.69	5.34	7.57
17	2018.04.09	1.36	3.57	6.18	5.75	5.62	7.54	45	2019.04.18	1.25	3.25	5.85	5.73	5.28	7.19
18	2018.04.17	1.61	3.66	6.16	5.73	5.85	7.61	46	2019.04.19	1.29	3.70	5.89	5.77	5.35	7.67
19	2018.04.18	1.26	3.50	6.14	5.75	5.49	7.46	47	2019.05.21	0.98	2.71	5.63	5.61	4.86	6.57
20	2018.05.09	1.78	3.28	6.11	5.76	5.99	7.25	48	2019.05.22	0.61	2.94	5.77	5.66	4.58	6.84
21	2018.05.10	1.58	2.53	6.08	5.74	5.77	6.93	49	2019.05.23	0.63	3.33	5.73	5.67	4.58	7.24
22	2018.06.06	1.56	2.92	6.03	5.70	5.72	6.85	50	2019.06.02	0.20	3.01	5.83	5.72	4.22	6.95
23	2018.06.07	0.17	2.46	6.03	5.86	4.33	6.50	51	2019.06.03	0.32	3.01	5.82	5.70	4.33	6.94
24	2018.06.11	0.43	2.50	6.01	5.77	4.57	6.47	52	2019.06.04	0.40	2.82	5.88	5.76	4.45	6.79
25	2018.06.12	0.42	2.11	6.04	5.79	4.58	6.10	53	2019.06.11	1.05	2.67	5.80	5.65	5.05	6.56
26	2018.06.13	0.53	2.29	6.00	5.79	4.67	6.27	54	2019.06.12	0.24	2.67	5.82	5.61	4.25	6.54
27	2018.06.15	0.19	2.05	5.99	5.84	4.31	6.08	55	2019.06.14	0.48	2.88	5.74	5.61	4.43	6.75
28	2018.10.29	0.97	2.96	6.02	5.69	5.12	6.88	56	2019.06.23	0.44	2.89	5.75	5.61	4.47	6.76

## References

- [1] Solar Heat Worldwide. International Energy Agency. <https://www.iea-shc.org/solar-heat-worldwide>.
- [2] Jing Li, Xiao Ren, Weiqi Yuan, Zhaomeng Li, Gang Pei, Yuehong Su, Kutlu Cagri, Jie Ji, Saffa Riffat. Experimental study on a novel photovoltaic thermal system using amorphous silicon cells deposited on stainless steel. *Energy* 2018; 159:786-798.
- [3] R. Platz, D. Fischer, M.A. Zufferey, J.A.A. Selvan, A. Haller, A. Shah. Hybrid collectors using thin-film technology. In: *Proceedings of 26th IEEE Photovoltaic Specialists Conference* 1997:1293-1296.
- [4] Virtuani A, Pavanello D, Friesen G. Overview of temperature coefficients of different thin film

1 photovoltaic technologies. In: 25th European photovoltaic solar energy conference and  
2  
3 exhibition/5th World conference on photovoltaic energy conversion 2010: 6-10.  
4

5  
6 [5] D.L. King, J.A. Kratochvil, W.E. Boyson. Temperature coefficients for PV modules and arrays:  
7  
8 measurement methods, difficulties, and results. In: Proceedings of 25th IEEE Photovoltaic  
9  
10 Specialists Conference 1997:1183-1186.  
11

12  
13  
14 [6] George Makrides, Bastian Zinsser, Alexander Phinikarides, Markus Schubert, George E.  
15  
16 Georghiou. Temperature and thermal annealing effects on different photovoltaic technologies.  
17  
18 Renewable Energy 2012; 43: 407-417.  
19

20  
21  
22 [7] Tetsuyuki Ishii, Kenji Otani, Takumi Takashima, Shinji Kawai. Estimation of the maximum power  
23  
24 temperature coefficients of PV modules at different time scales. Solar Energy Materials & Solar  
25  
26 Cells 2011; 95:386-389.  
27

28  
29  
30 [8] Xiao Ren, Jing Li, Mingke Hu, Gang Pei, Dongsheng Jiao, Xudong Zhao, Jie Ji. Feasibility of an  
31  
32 innovative amorphous silicon photovoltaic/thermal system for medium temperature applications.  
33  
34 Appl Energy 2019; 252: 113427.  
35

36  
37  
38 [9] M. Shima, M. Isomura, K. Wakisaka, K. Murata, M. Tanaka. The influence of operation  
39  
40 temperature on the output properties of amorphous silicon-related solar cells. Sol Energy Mater  
41  
42 Sol Cells 2005; 85:167-175.  
43  
44

45  
46  
47 [10]R. Ruther, G. Tamizh-Mani, J. del Cueto, J. Adelstein, M.M. Dacoregio, B. von Roedern.  
48  
49 Performance test of amorphous silicon modules in different climates-year three: higher minimum  
50  
51 operating temperatures lead to higher performance levels. In: Proceedings of 31th IEEE  
52  
53 Photovoltaic Specialists Conference 2005:1635-1638.  
54  
55

56  
57  
58 [11]J.A. del Cueto, B. von Roedern. Temperature-induced changes in the performance of amorphous  
59

1 silicon multi-junction modules in controlled light-soaking. Prog Photovolt Res Appl 1999; 7:101-  
2  
3 112.  
4

5  
6 [12]R. Ruther, J. del Cueto, G. Tamizh-Mani, A.A. Montenegro, S. Rummel, A. Anderberg, B. von  
7  
8 Roedern. Performance test of amorphous silicon modules in different climates-year four: Progress  
9  
10 in understanding exposure history stabilization effects. In: Proceedings of 33rd IEEE Photovoltaic  
11  
12 Specialists Conference 2008:1074-1079.  
13  
14

15  
16  
17 [13]J. Rozario, J.M. Pearce. Optimization of annealing cycles for electric output in outdoor conditions  
18  
19 for amorphous silicon photovoltaic–thermal systems. Appl Energy 2015; 148:134-414.  
20  
21

22  
23 [14]M.J.M. Pathak, J.M. Peace, S.J. Harrison. Effect on amorphous silicon photovoltaic performance  
24  
25 from high-temperature pulse in photovoltaic thermal hybrid devices. Sol Energy Mater Sol Cells  
26  
27 2012; 100:199-203.  
28  
29

30  
31 [15]D. E. Carlson, G. Lin. G. Ganguly. Temperature dependence of amorphous silicon solar cell PV  
32  
33 parameters. In: Proceedings of 28th IEEE Photovoltaic Specialists Conference 2000:707-712.  
34  
35

36  
37 [16]J.M. Pearce, J. Deng, M.L. Albert, C.R. Wronski, R.W. Collins. Room temperature annealing of  
38  
39 fast state from 1 sun illumination in protocrystalline Si:H materials and solar cells. In: Proceedings  
40  
41 of 31th IEEE Photovoltaic Specialists Conference 2005:1536-1539.  
42  
43

44  
45 [17]Anu Antony, Y.D Wang, A.P Roskilly. A detailed optimisation of solar photovoltaic/thermal  
46  
47 systems and its application. Energy Procedia 2019; 158: 1141–1148.  
48  
49

50  
51 [18]Ramos Cabal Alba, Guarracino Ilaria, Mellor Alexander, Alonso-Alvarez Diego, Ekins-Daukes  
52  
53 Nicholas, Markides Christos. Solar-thermal and hybrid photovoltaic-thermal systems for  
54  
55 renewable heating. Grantham Institute Briefing Paper, May 2017.  
56  
57

58  
59 [19]Lovedeep Sahota, G.N. Tiwari. Review on series connected photovoltaic thermal (PVT) systems:  
60

1 Analytical and experimental studies Sol Energy 2017; 150: 96-127.

2  
3 [20]G.N. Tiwari, R.K. Mishra, S.C. Solanki. Photovoltaic modules and their applications: A review on  
4 thermal modelling. Appl Energy 2011; 88: 2287-2304.  
5  
6

7  
8 [21]Ji Jie, Pei Gang, He Wei, Sun Wei, Li Guiqiang, Li Jing. Research progress on solar  
9 photovoltaic/thermal systems utilization. Science Press, Beijing; 2017.08. ISBN: 9787030539793.  
10  
11

12 [22]Pei Gang, Fu Huide, Ji Jie, Chow Tin-tai, Zhang Tao. Annual analysis of heat pipe PV/T systems  
13 for domestic hot water and electricity production. Energy Conversion and Management 2012; 56:  
14 8-21.  
15  
16  
17

18 [23]Wim G. J. van Helden, Ronald J. Ch. van Zolingen and Herbert A. Zondag. PV thermal systems:  
19 PV panels supplying renewable electricity and heat. Prog. Photovolt: Res. Appl. 2004; 12:415-  
20 426.  
21  
22

23 [24]Jean Zaraket, Michel Aillerie, Chafic Salame. Capacitance evolution of PV solar modules under  
24 thermal stress. Energy Procedia 2017; 119:702-708.  
25  
26  
27

28 [25]D.E. Carlson. Monolithic amorphous silicon alloy solar modules. Sol. Energy Mater. Sol. Cells  
29 2003;78: 627-645.  
30  
31

32 [26]R. Gottschalg, T.R. Betts, S.R. Williams, D. Sauter, D.G. Infield, M.J. Kearney. A critical appraisal  
33 of the factors affecting energy production from amorphous silicon photovoltaic arrays in a  
34 maritime climate. Sol. Energy 2004;77: 909-916.  
35  
36  
37

38 [27]C. Radue, E.E. van Dyk. A comparison of degradation in three amorphous silicon PV module  
39 technologies. Sol. Energy Mater. Sol. Cells 2010; 94: 617-622.  
40  
41  
42

43 [28]Xunlight Corporation. [www.xunlightchina.com](http://www.xunlightchina.com), 2015.2.  
44  
45

46 [29]ANSI/ASHRAE 93-2010 Methods of testing to determine the thermal performance of solar  
47  
48  
49

collectors. New York: ASHRAE; 2010.

- [30] Jie J, Jianping L, Chow TT, Wei H, Gang P. A sensitivity study of a hybrid photovoltaic/thermal water-heating system with natural circulation. *Appl Energy* 2007; 84: 222-237.
- [31] Maysam Gholampour, Mehran Ameri. Energy and exergy analyses of Photovoltaic/Thermal flat transpired collectors: Experimental and theoretical study. *Appl Energy* 2016; 164: 837-856.
- [32] Jeter SM. Maximum conversion efficiency for the utilization of direct solar radiation. *Sol Energy* 1981; 26: 231–6.
- [33] M. Nikolaeva, R.P. Kenny, E. Dunlop, M. Pravettoni. Seasonal variations on energy yield of a-Si, hybrid, and crystalline Si PV modules. *Prog Photovolt Res Appl* 2010; 18:311-320.
- [34] A. Virtuani, L. Fanni. Seasonal power fluctuations of amorphous silicon thin-film solar modules: Distinguishing between different contributions. *Prog Photovolt Res Appl* 2014; 22:208-217.
- [35] G. Evola, L. Marletta. Exergy and thermoeconomic optimization of a water-cooled glazed hybrid photovoltaic/thermal (PVT) collector. 2014; 107: 12-25.
- [36] Kołodziej, A. Staebler-Wronski effect in amorphous silicon and its alloys. *Opto-Electronics Review* 2004; 12 (1): 21–32.

## Credit author statement

**Xiao Ren:** Conceptualization, Methodology, Software, Validation, Writing - original draft, Writing - review & editing.

**Jing Li:** Supervision, Conceptualization, Methodology, Resources, Writing - original draft, Writing - review & editing.

**Dongsheng Jiao:** Methodology, Formal analysis, Software.

**Datong Gao:** Investigation, Data curation.

**Gang Pei:** Supervision, Methodology, Funding acquisition, Resources, Writing - review & editing.